# Single-electron capture in intermediate energy $He^{2+}$ + He collisions

Ting Cao[1,2], Junwen Gao[3], Yong Gao[2,4], Shuncheng Yan[2,4], Xiaolong Zhu[2,4], Ruitian Zhang[2,4], Dalong Guo[2,4], Kaizhao Lin[2,4], Xiaoxia Wu[2,4], Shaofeng Zhang[2,4],* and Xinwen Ma [2,4]†

[1]*College of General Education, Shanxi College of technology, Shuozhou 036000, China*
[2]*Institute of Modern Physics, Chinese Academy of Sciences, Lanzhou 730000, China*
[3]*School of Physics, Hangzhou Normal University, Hangzhou 311121, China and*
[4]*University of Chinese Academy of Sciences, Beijing 100049, China*

(Dated: September 19, 2026)

A combined experimental and theoretical study on single-electron capture in 30 − 125 keV/u $He^{2+}$ + He collisions was performed. Single-electron capture state-selective and angular-differential cross sections were measured using a cold target recoil ion momentum spectroscopy, for which the longitudinal momentum resolution has been improved up to 0.066 a.u.. More details of electron captured to higher excited-states and transfer-excitation processes were obtained from angular-differential cross sections. It was found that the experimental angular-differential cross sections were in good agreement with the two-active-electron semiclassical asymptotic-state close-coupling calculation for the considered impact energies. It is shown that single electron capture mainly occurs at small projectile scattering angles (< 0.4 mrad), where prominent oscillatory structures resulting from Fraunhofer-type diffraction can be seen. While a significant contribution from large projectile scattering angles (> 0.6 mrad) was observed in the transfer-excitation process at 30 keV/u. From a quasi-molecular interaction picture, it is shown that both the small internuclear distance radial coupling and rotational coupling at the united-atom limit are responsible for the large angle scattering mechanism at 30 keV/u.

PACS numbers: 34.10.+x, 34.80.Dp
Keywords: cold target recoil ion momentum spectroscopy, ion-atom collisions, electron capture, angular-differential cross sections

## I. INTRODUCTION

Electron capture (EC) occurring in ion-atom collisions is a process in which one or more target electrons are transferred from the neutral atom into the moving projectile ion [1, 2]. The potential role of EC processes has attracted widespread attention from scientists in different fields, such as astrophysics and radiobiology. For the former, the discovery of comet X-ray emission is caused by the EC process between solar wind ions and neutral species on the comet [3–7]. For the latter, the detailed knowledge of cross sections are needed to feed statistical methods that track the energy deposition[8]. Furthermore, the study of EC processes can also provide valuable information about the atomic structure [9, 10] and few-body dynamic mechanism [11].

In view of these important aspects, the single-electron capture (SEC) process, in particular, charged particles colliding with helium, has been given much attention in both experimental [12–17] and theoretical [18–21] aspects over the past decades, respectively. In this work, we are interested in $He^{2+}$ + He collisions, such collision system is also of challenging importance in relation to the effects of the electronic correlation between the two active electrons of the target in the collision process. However, most previous experimental [22–26] and theoretical [27–34] investigations focused mainly on the energy dependence of total SEC cross sections.

Experimentally, Afrosimov *et al.* [35] and Folkerts *et al.* [36] performed state-selective SEC cross sections measurements using energy gain spectroscopy and photon emission spectroscopy respectively, for energies ranging from 0.5 to 15 keV/u and 1 to 75 keV/u, respectively. However, energy gain spectroscopy has been used only in slow ion-atom collisions, necessitating a high-quality ion beam to achieve the desired resolution. The typical energy resolution of energy gain spectroscopy reached is about $\Delta Q/E_P = 10^{-4}$ [37]. While the photon emission spectroscopy method offers high resolution without restrictions on ion beam energy and quality, it faces constraints in measuring reaction channels that do not emit photons, such as electron capture to the ground state. Additionally, its experimental efficiency is diminished due to the restricted solid angle ($10^{-4}$ – $10^{-3}$ of $4\pi$). Later in the 1990s, with the advent of the cold target recoil ion momentum spectroscopy (COLTRIMS) method, several laboratories worldwide has led to an important advance in the experimental studies of atomic and molecular collisions. This method can perform measurement of ion-atom collision at the fully differential level, and provide an unprecedented kinematically complete physical picture for collision processes to shed more light on the basic reaction dynamics [38, 39]. Using COLTRIMS technique, Mergel *et al.* [37], Schöffler *et al.* [40] and Alessi *et al.* [41] have measured state-selective and angular-differential SEC cross sections in $He^{2+}$-He collisions for impact energies 0.25 - 1 MeV, 60 - 630 keV/u and 13.3 - 100 keV/u, respectively. During the past 10 years, Zhu *et al.* [42] and Wang *et al.* [43] also measured state-selective and angular-differential SEC cross sections in $He^{2+}$-He collisions for low energy in 7.5 keV/u and 10 - 17.5 keV/u, respectively. However, due to the limitation of the experimental resolution in Ref. [37, 41, 42], $n$-selective electron capture processes can not be fully resolved, the obtained state selective and angular-differential cross sections summed over a number of excited states of projectile or target may wash out the structure in

* zhangshf@impcas.ac.cn
† x.ma@impcas.ac.cn

the individual channels and obscure the comparison to theory. In addition, the authors mainly attention is addressed to the angular-differential cross sections for SEC to $He^+(1s)$ of $He^{2+}$-He collisions in Ref. [40, 43].

In this work, we present experimental findings from the collision of $He^{2+}$ ions with He atoms at projectile energies ranging from 30 − 125 keV/u. Using the COLTRIMS technique with an improved resolution up to 0.066 a.u., we were able to determine the relative state-selective cross sections and angular-differential cross sections of the collision with $n$-resolution at intermediate projectile energies. The mechanisms underlying the structures observed in the angular-differential cross sections of ground-state transfer, transfer to excited, and transfer-excitation processes, which were indistinguishable in early experiments, have also been discussed. The present angular-differential cross sections obtained compared further with the theoretical calculations using a semiclassical asymptotic-state close-coupling (SCASCC) approach to provide physical insight into this collision system.

The paper is organized as follows. The experimental setup is shown in Sec. II. We briefly outline the SCASCC approach used in the present calculations in Sec. III. Section IV is devoted to the detailed analysis of relative state-selective cross sections and angular-differential cross sections. Followed by the conclusions in Sec. V.

## II. EXPERIMENTAL SETUP

The experiment was conducted at the 320-kV platform for multidisciplinary research with highly charged ions at the Institute of Modern Physics, Chinese Academy of Sciences, Lanzhou, China [44, 45]. The $He^{2+}$ beam produced in the 14.5-GHz electron cyclotron resonance ion source (ECRIS) was extracted, magnetically charge analyzed, and then accelerated to the desired energy. Before the beam entering the collision chamber, two sets of mutually perpendicular and adjustable slits are installed at a distance of 1m from the collision zone to collimate the beam to a size of $0.5\times0.5$ mm$^2$. Several sets of electrostatic deflectors installed in front of the collision chamber were used to steer the beam to the target and to clean charge-state impurities from the beam.

As shown in Fig. 1, a newly built COLTRIMS is installed at a dedicated beam line for atomic collisions studies. The working principle of the COLTRIMS detecting technique has been described in Refs. [38, 39]. But in this experiment, as shown in the Fig. 1, a new time-of-flight (TOF) spectrometer have been used[46, 47]. In the target chamber, the $He^{2+}$ beam passing through a small hole with a diameter of 20 mm on one side of the TOF electrodes intersected with a supersonic gas jet which consisted of two stages of a differential vacuum system. The lengths of the accelerating zone of the TOF were 380 mm without the one-dimensional time focusing geometry (Wiley-McLaren time focusing condition) [48]. In order to minimize the influence of the finite interaction volume on the momentum resolution, we used an adjustable slits to collimate the gas jet to a size of 0.5 mm in the direction of $He^{2+}$ beam at the intersection. The gas jet expanded through a 30 $\mu$m nozzle from a gas reservoir and extracted through two skimmers with a size of 0.3 mm and 0.5 mm in diameter, and then entered to the target chamber. The typical density of the gas target was estimated to be $5\times10^{10}$ atoms/cm$^2$ at the intersection with a driving pressure of 20 bar. In the direction with an angle of 14 degrees to the $He^{2+}$ beam, we applied a weak homogeneous electrostatic field of 0.85 V/cm to project the recoil ions onto a position sensitive detector (PSD) of 75 mm diameter. To maximize the acceptance efficiency for electrons, a homogeneous magnetic field of 6.0 G parallel to the electrostatic field generated by a pair of Helmholtz coils was used. Scattered ions (the neutral He and the $He^+$) were separated from the $He^{2+}$ beam by an electrostatic deflector downstream of the target chamber and detected by a PSD about 1.8 m downstream of the target zone. The residual projectile beam is collected by a Faraday cup.

For capture reactions in the ion-atom collisions, the longitudinal momentum vector of the recoil ion $P_z$ (parallel to the projectile beam axis) follows

$$P_z = -\frac{Q}{v_p} - \frac{nv_p}{2}, \tag{1}$$

where $v_p$ is the projectile velocity, $n$ is the number of electrons captured from the target to the projectile, and $Q$ is the binding energy difference of the active electron before and after collision and defined as,

$$Q = \epsilon_i - \epsilon_f \tag{2}$$

where $\epsilon_i$ and $\epsilon_f$ are binding energy of the active electron in the initially ground-state target and finally excited ion, respectively. Owing to the quantization of $Q$ value, the recoil ion momentum is discrete. Therefore, for certain projectile energy, the $Q$ value can be obtained from $P_z$, and then the distribution of state-selective population after the collision can be obtained. From the momentum conservation, the transverse momentum of the recoil ion $P_{xy}$ (perpendicular to the projectile beam axis) equals the loss of projectile momentum in the transverse direction, and is related to the projectile scattering angle $\theta$ as

$$P_{xy} = -P_0 \tan\theta, \tag{3}$$

where $P_0$ is the projectile momentum.

For suppressing the contamination form other processes, measurement has been carried out with double coincidence between recoil ions and scattered projectile. The projectile scattering angle differential cross sections of different reaction channels are obtained by choosing the events of different $P_z$ in the data analysis system. The momentum resolution was estimated to be 0.4 a.u. in $x$ direction (target beam direction) and 0.03 a.u. in $y$ direction (perpendicular to the directions of target and projectile beam) and 0.07 a.u. in $z$ direction (projectile beam direction) (see Fig. 1). With the present setup, it has been reported that the longitudinal momentum-resolution is about 5-6 times better than the previous one with the transversal extraction mode [49, 50]. Note that, in order to collect recoil ions with greater transverse momentum, increasing the

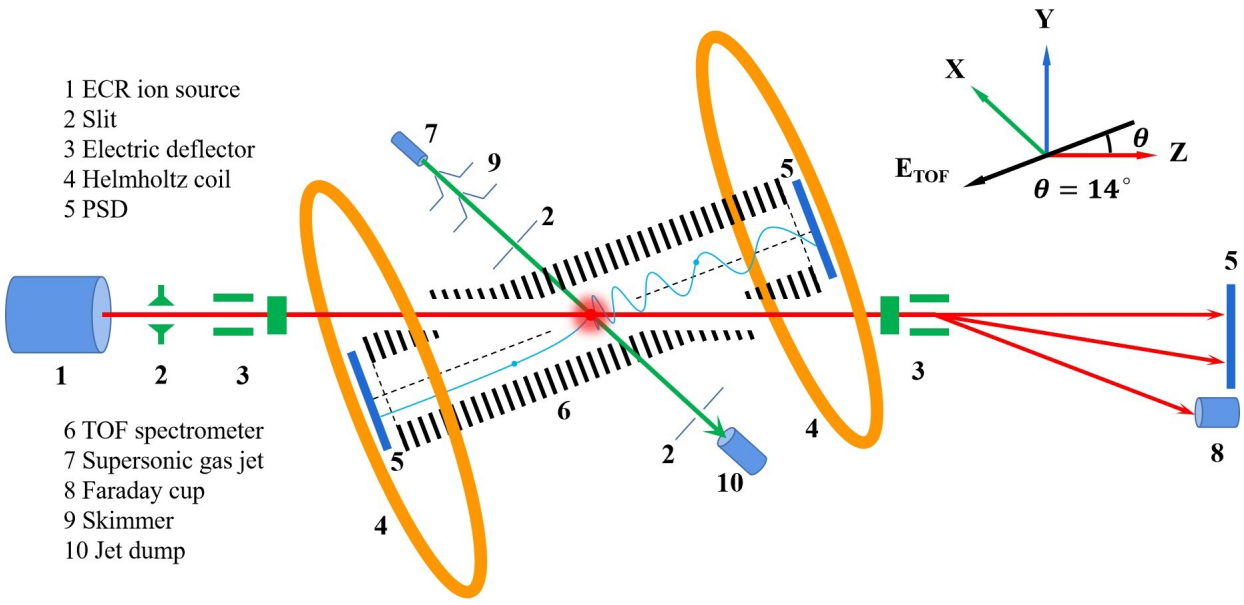



FIG. 1. (Color online) An overview of the newly built COLTRIMS experimental setup at the 320-kV platform for research with highly charged ions.

TOF voltage will lead to an increase in longitudinal momentum resolution (see Fig. 2(a) and Fig. 7(a)). The statistical error bars were simply calculated by a square root of event counts. Atomic units are used throughout this paper unless other wise stated.

## III. THEORETICAL METHOD

In the present work, the cross sections of the EC processes occurring during $He^{2+}$ + He collisions are calculated using a two-active-electron semiclassical asymptotic-state close-coupling (SCASCC) approach which has been previously described, for example in Ref. [51–53]. We only outline here briefly the main features of the approach. The two-electron time-dependent Schrödinger equation (TDSE) is written as

$$\left[H - i\frac{\partial}{\partial t}\right]\Psi(\vec{r}_1, \vec{r}_2, t) = 0, \tag{4}$$

with the electronic Hamiltonian,

$$H = \sum_{i=1,2}\left[-\frac{1}{2}\nabla_i^2 + V_T(r_i) + V_P(r_i^p)\right] + \frac{1}{|\vec{r}_1 - \vec{r}_2|}, \tag{5}$$

and $\vec{r}_i$, $\vec{r}_i^{\,p} = \vec{r}_i - \vec{R}(t)$ are the position vectors of the electrons with respect to the target and the projectile respectively. The relative projectile-target position $\vec{R}(t)$ defines the trajectory, with $\vec{R}(t) = \vec{b} + \vec{v}_P t$ in the usual straight-line, constant velocity approximation where $\vec{b}$ and $\vec{v}_P$ are the impact parameter and velocity respectively. In the present collision system, the potentials $V_T = -2/r_i$ and $V_P = -2/r_i^p$ describe the interaction between the electrons and the target (He) and projectile ($He^{2+}$) nucleus.

The Schrödinger equation is solved by expanding the wave-function $\Psi$ accordingly on a set of electronic states described with Gaussian-type orbitals (GTOs) and spin-adapted products of these GTOs centred on both isolated collision partners. Furthermore, they are augmented with plane-wave electronic translation factors to ensure Galilean invariance of the results. The probability amplitudes $a_f$ for a given final state $f$ included in the expansion are obtained after propagation of the initial state $i$, and the integral cross sections can be evaluated through,

$$\sigma_{fi}(v_P) = 2\pi \int_0^{+\infty} bP_f(b, v_P)db, \tag{6}$$

with the transition probability $P_f(b, v_P) = |a_f(b, v_P)|^2$.

In the same manner as in [49, 54, 55], the angular-differential cross sections for inelastic processes are expressed in the center of mass frame as,

$$\begin{aligned}\frac{d\sigma_{fi}}{d\Omega} &= \left|f_{fi}(\theta, \phi)\right|^2 \\ &= \left|\mu v(-i)^{1+|\Delta m_{fi}|}e^{-i\Delta m_{fi}\phi}\right. \\ &\times \left.\int_0^{\infty} bdbJ_{|\Delta m_{fi}|}(2\mu v b sin(\theta/2))c_f(b, v_P)\right|^2\end{aligned} \tag{7}$$

where the scattering amplitude $f_{fi}$ is given as a Bessel transform of the collision amplitude $c_f$, $\mu$ is the reduced mass of the target and projectile, $\Delta m_{fi} = m_f - m_i$ with $m_i$, $m_f$ are the magnetic quantum numbers of the initial and final states, respectively. It should be noted that all $b$-dependent phases should be included in the collision amplitudes $c_f(b, v_p)$ of Eq. 7. This implies the inclusion of the common phase related to the core-core Coulomb interaction [56], which can be factorized out from the total Hamiltonian by a trivial phase transform to get

to the Hamiltonian written in Eq. 5. From the amplitude $a_f$ obtained by solving the TDSE in a large, but finite, time domain, the collision amplitude can then be expressed as

$$c_f(b, v_P) = a_f(b, v_P) \exp\Big(\frac{i}{v_P} 2Z^T Z^P ln b\Big), \tag{8}$$

where $Z^T$ and $Z^P$ are respectively the target and projectile charges ( 2 for both of them in the present system). It is indeed the complete phase information that allows the extraction of the angular differential cross sections from straight-line trajectory collision amplitudes.

In the present calculations, a set of 49 Gaussian-type orbitals (GTOs) (10 for $l = 0$, $8 \times 3$ for $l = 1$ and $3 \times 5$ for $l = 2$) are used on both projectile and target centers; this allows the inclusion of 1897 singlet states in total : 555 TT (states of two electrons on target), 555 PP (states of two electrons on projectile), and 787 TP ($He^+$, $He^+$) singlet states. The cross sections reported in the following have been compared with those obtained with a smaller basis set built from 36 GTOs (8 for $l = 0$, $6 \times 3$ for $l = 1$ and $2 \times 5$ for $l = 2$) for both projectile and target. The angular-differential cross sections for ground-state transfer (GT) and transfer to excited-state (ET) from these two sets agree with each other within 9% for the considered energies. For transfer-excitation (TE) processes, the DCS converged within 35% at worse at 30 keV/u, 15% at intermediate energies and to be better than 6% for highest energies we considered (125 keV/u).

## IV. RESULTS AND DISCUSSION

The SEC process can take place via the following three reaction channels:

$$\begin{aligned} He^{2+} + He &\rightarrow He^+(n = 1) + He^+(n = 1) \qquad \text{(GT)}, \\ &\rightarrow He^+(n \geq 2) + He^+(n = 1) \\ &\;\;\& \; He^+(n = 1) + He^+(n' \geq 2) \qquad \text{(ET)}, \\ &\rightarrow He^+(n \geq 2) + He^+(n' \geq 2) \qquad \text{(TE)}, \end{aligned} \tag{9}$$

where GT corresponds to ground-state transfer; ET denotes the transfer to excited-state process in which one electron is captured into projectile excited states while the second one is kept on the target ground state (or one electron is captured into the projectile ground state and the second one on the target is excited); TE represents the transfer-excitation process that captures one electron into projectile excited state while excites the second one on the target.

The measured recoil-ion longitudinal momentum distributions for SEC by $He^{2+}$ from He at impact energies of 30, 62.5 and 125 keV/u are shown in Fig. 2. In order to extract the state-selective cross sections, the longitudinal recoil-ion momentum distributions have been fitted with Gaussian functions. The different peaks correspond to different final states indicated by $(n, n')$. In this notation, $n$ denotes the individual quantum number of the captured electron and $n'$ denotes the individual quantum number of electron which remains bound to the target. When the reaction products are symmetric, like

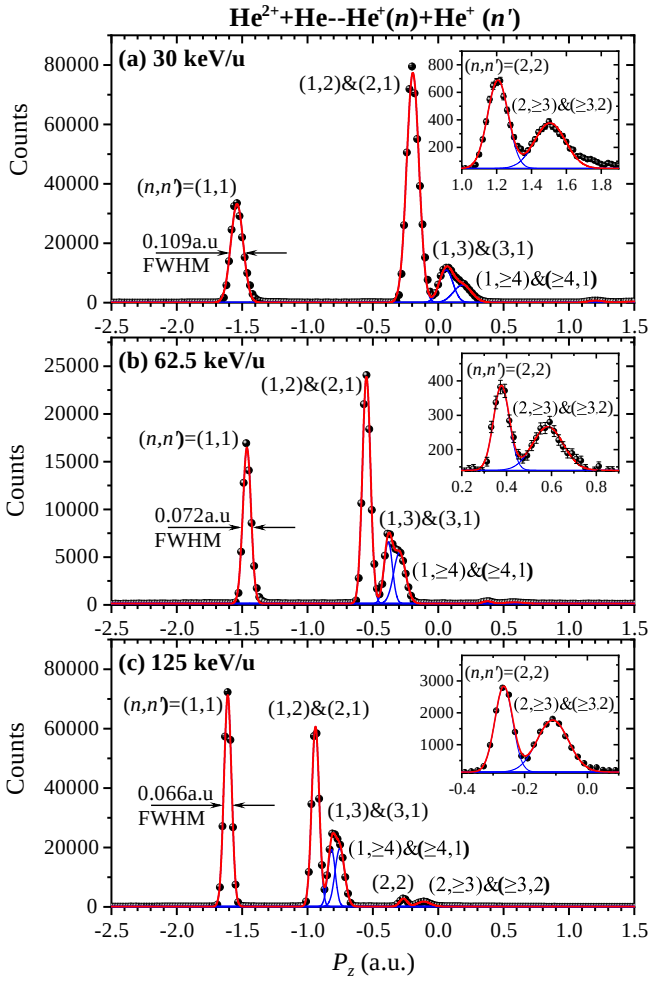



FIG. 2. (Color online) Recoil-ion longitudinal momentum distributions for SEC from He in collision with $He^{2+}$ at (a) 30, (b) 62.5 and (c) 125 keV/u, respectively. Solid circles: experimental measurements. Solid curves: Gaussian fittings. Each inset plot shows more detailed momentum distribution of TE process.

in the $(1, 2)\&(2, 1)$ processes, their experimental separation becomes very challenging. Therefore, for $n = 2$, the experiments provide data for the sum of the cross sections for electron capture and residual target-ion excitation into the corresponding shell (see Eq. 9).

In particular, the relative state-selective cross sections were extracted from the corresponding fitting curves shown in Fig. 2 and these values are listed in Table I. Clearly, at higher impact energy of 125 keV/u, the spectrum indicates that the GT process is overwhelmingly dominant over the other processes. Fitting the peak $(1, 1)$, corresponding to the GT process, reveals a remarkable recoil ion longitudinal momentum resolution of 0.066 atomic units. Besides the dominant reaction channel, the contributions from the ET and TE processes can also be identified at present longitudinal momentum resolution. Compared with earlier experimental results [37, 41, 42], the present experimental results can further distinguish the $(1, 3)\&(3, 1)$ and $(1, \geq 4)\&(\geq 4, 1)$ from $(1, \geq 3)\&(\geq 3, 1)$,

TABLE I. Present experimental relative state-selective cross sections $\sigma_{rel}$ (%) for $He^{2+}$-He collisions. (Errors given in the bracket are determined from Gaussian fitting error of the peak.)

| Final state $(n, n')$ | Energy (keV/u) | | |
|---|---|---|---|
| | 30 | 62.5 | 125 |
| (1,1) | 25.18 (0.76) | 29.92 (0.72) | 39.38 (0.61) |
| (1,2)&(2,1) | 58.15 (1.37) | 42.87 (0.96) | 33.38 (0.53) |
| (1,3)&(3,1) | 9.13 (0.44) | 12.02 (0.59) | 10.49 (0.69) |
| $(1, \geq 4)\&(\geq 4, 1)$ | 6.47 (0.43) | 14.18 (0.63) | 13.70 (0.74) |
| (2,2) | 0.61 (0.35) | 0.51 (0.24) | 1.47 (0.09) |
| $(2, \geq 3)\&(\geq 3, 2)$ | 0.47 (0.34) | 0.51 (0.33) | 1.57 (0.11) |

and likewise for the $(2, 2)$ and $(1, \geq 4)\&(\geq 4, 1)$ from $(2, \geq 3)\&(\geq 3, 2)$. As the impact energy decreases, the ET process $(2, 1)\&(1, 2)$ begins to gradually increase, and the TE process $(\geq 2, \geq 2)$ will become a more negligible contribution.

To get a better understanding, differential scattering angle distributions were unfolded for the $(1, 1)$, $(1, 2)\&(2, 1)$, $(1, 3)\&(3, 1)$, $(1, \geq 4)\&(\geq 4, 1)$ and $(2, 2)$ capture process, respectively. As shown in Fig. 3(a)-(c), we present the measured angular distributions for GT processes at impact energies 30, 62.5 and 125 keV/u, respectively. The present SCASCC results are also shown in the same figure for comparison. It can be observed that the measured angular differential cross section displays an oscillatory structure for all three impact energies.

Comparing with the theoretical results, good overall agreement is obtained, in particular, the oscillatory structure observed in the angular differential cross section is well reproduced by the theory. It can be seen from Fig. 3 that the structures move towards small scattering angles and get closer with each other for increasing impact energies. Due to the limitation of transversal momentum resolution, it is easy to understand that the discrepancy between the minima and maxima in present experimental and theoretical increases with the increase of collision energy. Such oscillatory structure has been observed in the past and interpreted as resulting from Fraunhofer-type diffraction [43, 50, 57–61]: the angular-differential cross sections present alternately minima and maxima like the diffraction pattern in optics, with alternately dark and bright fringes, where the first dark and bright fringes locates at

$$\begin{aligned} \theta_{min} &= 0.61\lambda/\rho, \\ \theta_{max} &= 0.819\lambda/\rho, \end{aligned} \tag{10}$$

in the case of a circular aperture of radius $\rho$, of a radiation of wavelength $\lambda$, see Ref. [62].

Using the analogy of Fraunhofer diffraction of electromagnetic radiations and *de Broglie* atomic scattering waves with $\lambda = 2\pi/\mu v_P$, and taking the aperture radius from the effective impact parameter range where electron transitions take place from the present SCASCC calculations, one can obtain the expected positions of the first dark and the first bright fringes. First, the positions of the 1st minimum $\theta_{dark}$, marked as black arrows in Fig. 3, are determined directly from the experimental cross sections. Second, from these minimum, an effective aperture radius $\rho$ is obtained so that the position of the first expected Fraunhofer bright fringe $\theta_{bright}$ is evaluated (see Eq. 10). In Table II, the values of our calculated effective aperture radius and the positions of first bright fringe are shown, the latter are also marked in Fig. 3 as red arrows. It can be seen in Table II and in Fig. 3 that for the three energies under consideration, the positions of the first maximum in our cross sections agree with the predicted positions stemming from the Fraunhofer-type diffraction model.

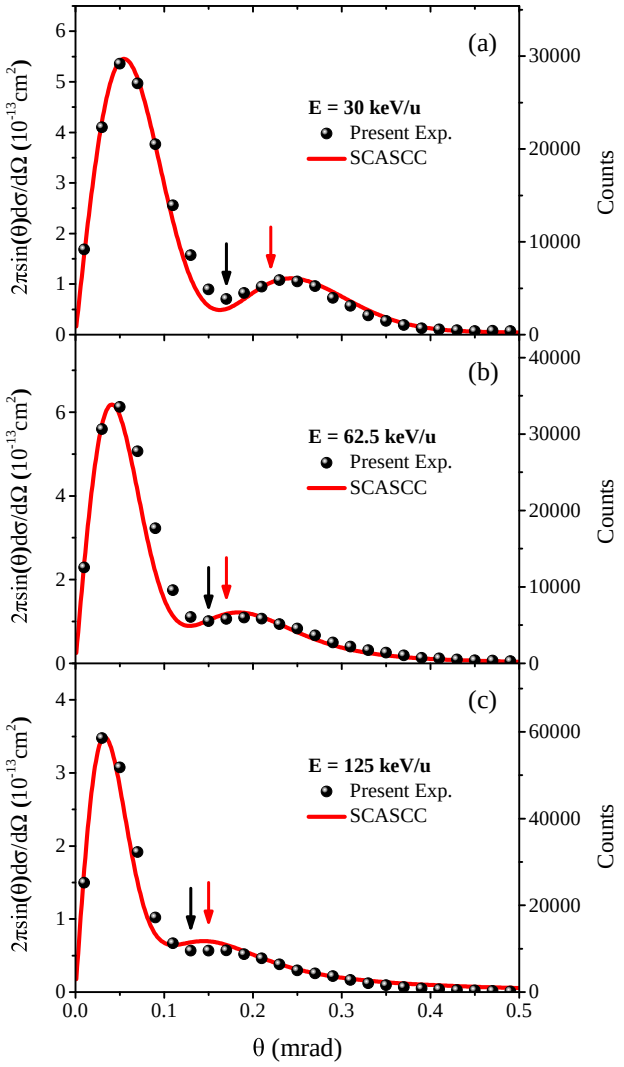



FIG. 3. (Color online) Angular-differential cross sections for GT process as functions of the laboratory scattering angles for (a) 30, (b) 62.5, and (c) 125 keV/u $He^{2+}$-He collisions. Solid symbols: present measurements; red curves: present SCASCC results. The error bars are smaller than the size of the data symbols. The black arrows show the positions of the first minimum in our angular-differential cross sections; the red arrows show the positions of the first bright fringe calculated by the Fraunhofer-type diffraction model.

To compare our calculated effective aperture radius with the corresponding effective impact parameter range, the probabilities of the GT process as a function of impact parameter are shown in Fig. 4 for impact energies 30, 62.5 and 125 keV/u. Our calculated effective aperture radius for the correspond-

TABLE II. Positions of the first minimum and maximum in the angular-differential cross sections of GT process as well as the effective aperture radius $\rho$ and the positions of the first bright fringe calculated by the Fraunhofer-type diffraction model.

| Energy (keV/u) | wavelength $\lambda$ (a.u.) | 1st minimum (mrad) | $\rho$ (a.u.) | 1st maximum (mrad) | 1st bright fringe (mrad) |
|---|---|---|---|---|---|
| 30 | 0.000781 | 0.17 | 2.8 | 0.23 | 0.22 |
| 62.5 | 0.000541 | 0.15 | 2.2 | 0.19 | 0.17 |
| 125 | 0.000383 | 0.13 | 1.8 | 0.17 | 0.15 |

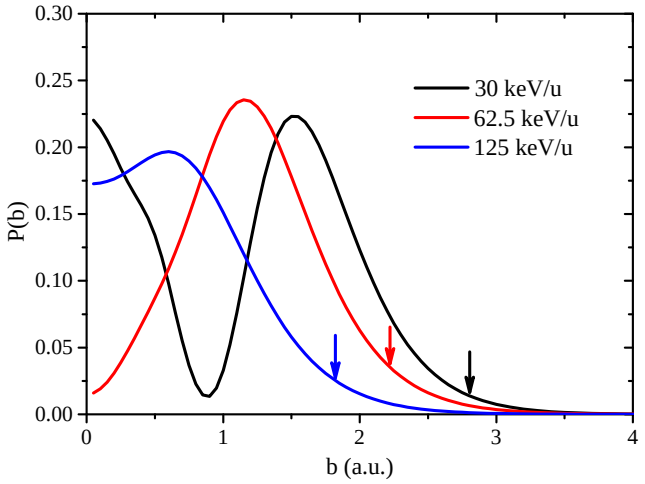



FIG. 4. (Color online) Transition probabilities of the GT process as functions of impact parameters and for three different impact energies. The arrows mark the positions of the effective aperture radius calculated by the Fraunhofer-type diffraction model, see Table II.

ing impact energies are denoted as arrows in the same figure. It is found that the probabilities of all these impact energies are negligibly small beyond the corresponding positions of the arrow. The effective impact parameter range is therefore in good agreement with the effective aperture radius. This tends to indicate that the oscillatory structure appearing in the GT angular-differential cross sections originates mainly from Fraunhofer-type diffraction.

Comparing to previous experimental studies [37, 40–43], the improved resolution in the present experiment allows the extraction of angular distributions for electron capture to higher excited states. In Fig. 5(a)-(c), we show the present experimental cross sections for ET to $(1,2)\&(2,1)$ state, together with the present SCASCC calculations for comparison. Excellent agreements can be obtained for all the considered impact energies. The theoretical results for ET to $(1s,2s)\&(2s,1s)$ and $(1s,2p)\&(2p,1s)$ states are also displayed in the same figure. Compared to the GT process, a similar behavior was observed, though with a weaker second peak. The oscillations for the $(1s,2s)\&(2s,1s)$ and $(1s,2p)\&(2p,1s)$ state, similar to $(1,1)$ state, may be also attributed to the Fraunhofer-type diffraction. The previous study revealed that the diffraction appears in electron capture for $\Delta m_l = 0$ [49]. In the present case, a similar process maybe occur for the $(1s,2p)\&(2p,1s)$ state, in which electron capture into the $2p$ state tends to occupy the orbit of $m_l = 0$. Furthermore, our SCASCC calculations show that the cross sections for ET to

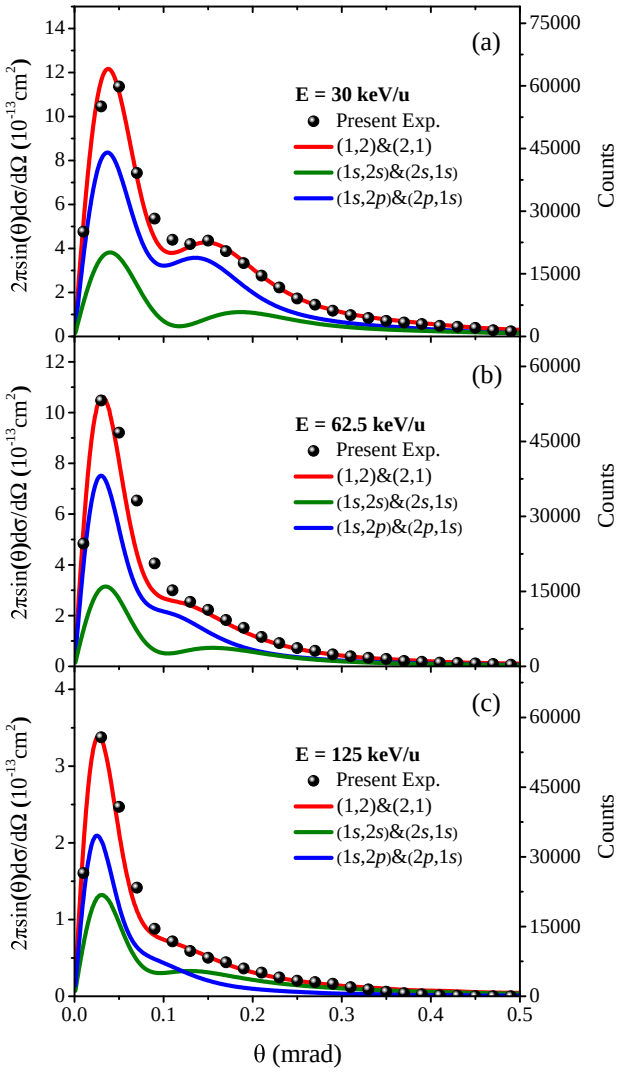



FIG. 5. (Color online) Angular-differential cross sections for $(1,2)\&(2,1)$ state of ET process as functions of the laboratory scattering angles for (a) 30, (b) 62.5, and (c) 125 keV/u $He^{2+}$-He collisions. Solid symbols: Present measurements; red curves: $(1,2)\&(2,1)$ state of SCASCC results; green curves: $(1s,2s)\&(2s,1s)$ state of SCASCC results; blue curves: $(1s,2p)\&(2p,1s)$ state of SCASCC results. The error bars are smaller than the size of the data symbols.

$(1s,2p)\&(2p,1s)$ is preferred at 30 keV/u, while as increasing impact energies, the ones for ET to $(1s,2s)\&(2s,1s)$ at large scattering angle become dominant.

In Fig. 6, we compare the present experimental cross sec-

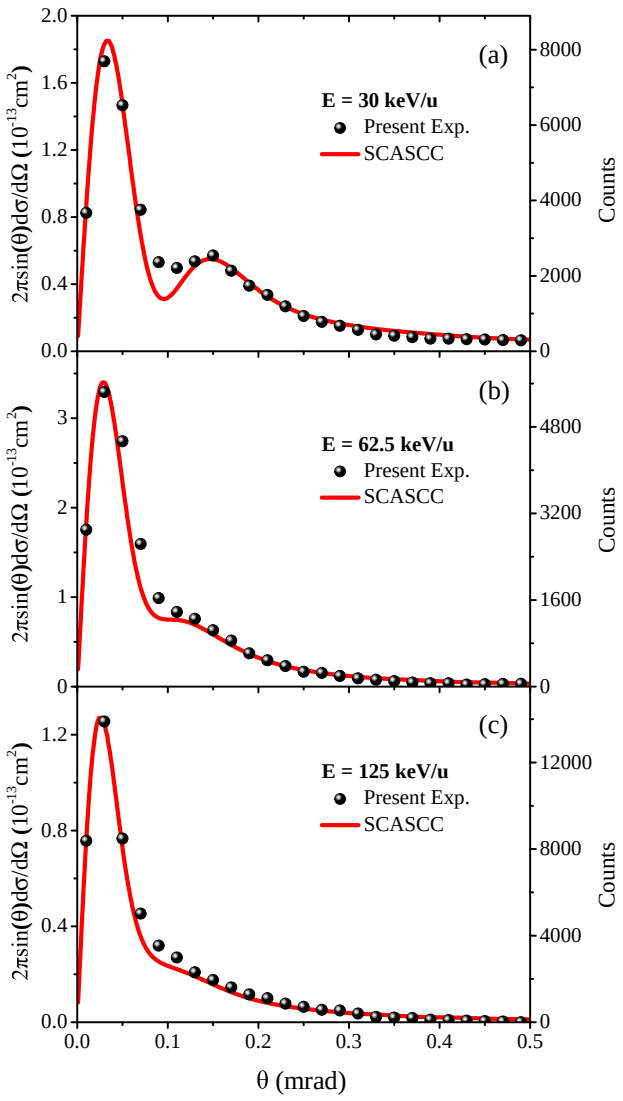



FIG. 6. (Color online) Angular-differential cross sections for $(1,3)\&(3,1)$ state of ET process as functions of the laboratory scattering angles for (a) 30, (b) 62.5, and (c) 125 keV/u $He^{2+}$-He collisions. Solid symbols: Present measurements; red curves: SCASCC results. The error bars are smaller than the size of the data symbols.

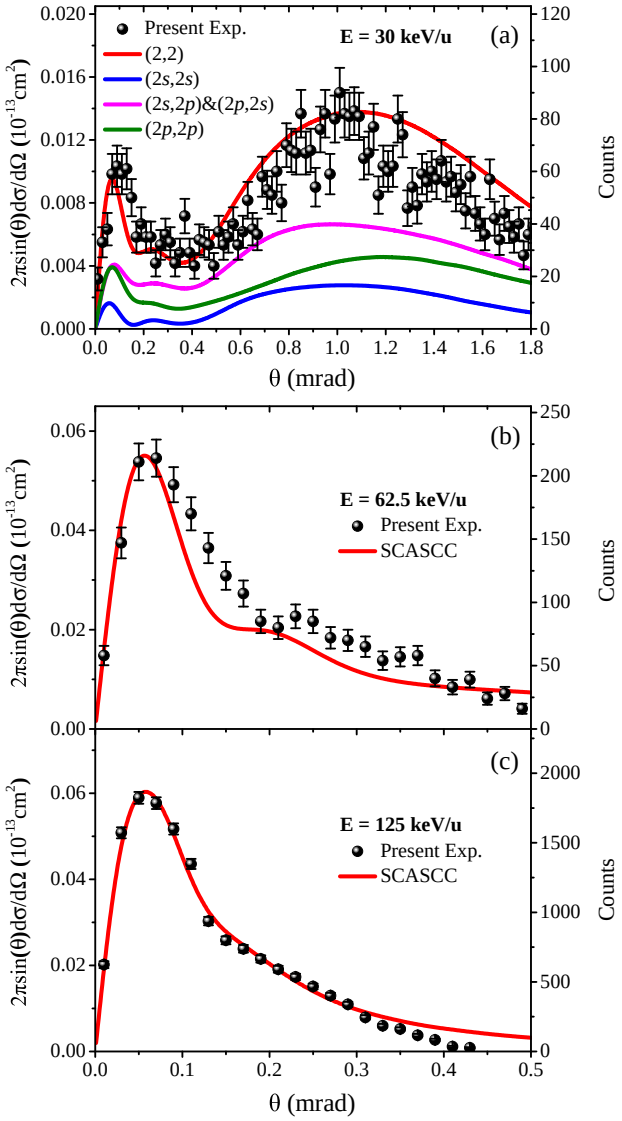



FIG. 7. (Color online) Angular-differential cross sections for $(2,2)$ state of TE process as functions of the laboratory scattering angles for (a) 30, (b) 62.5 and (c) 125 keV/u $He^{2+}$-He collisions. Solid symbols: Present measurements; red curves: SCASCC results. In Fig. 7(a), we also present the angular-differential cross sections of $(2s,2s)$ (blue curves), $(2s,2p)\&(2p,2s)$ (magenta curves) and $(2p,2p)$ (green curves) states.

tions for ET to $(1,3)\&(3,1)$ state with the present SCASCC calculations, showing again good agreements for all the considered impact energies. The cross sections display a similar behavior with the ones for ET to lower electronic states, as shown in Fig. 3 and 5.

The measured cross sections for TE to $(2,2)$ state are shown in Fig. 7(a)-(c) for impact energies 30, 62.5 and 125 keV/u, together with the SCASCC circulations for comparison. Good overall agreement is found between the present experimental data and SCASCC calculations, though, at 62.5 keV/u, less satisfactory than that in GT and ET processes. It is shown in Fig. 3, 5 and 6 that the GT and ET processes mainly occur at small projectile scattering angles (< 0.4 mrad), while in Fig. 7(a) the angular distribution for the TE process is dominated by large scattering angles (> 0.6 mrad) at 30 keV/u, and as increasing impact energies the contribution of the large scattering angles decreases and disappears from the cross sections. In fact, such significant contribution from large projectile scattering angles for TE process in $He^{2+}$ + He collisions was observed at low energies in the past [35, 63]. From a quasimolecular interaction picture (see Fig. 4 in Ref. [63] and corresponding text), the large angle scattering mechanism was attributed by Afrosimov *et al.* [35] to a small internuclear distance radial coupling between the incoming channel $2p\sigma_u^2\ ^1\Sigma_g$ (correlated asymptotically to $He^{2+}$ + $He(1s^2)$) and the outgoing channel $2s\sigma_g^2\ ^1\Sigma_g$ (correlated asymptotically to $He^+(2s)$ + $He^+(2s)$). Instead, Bordenave-Montesquieu *et al.* [63] at-

tributed it to a rotational coupling $\Sigma_g$-$\Pi_g$-$\Delta_g$ at the united-atom limit $Be^{2+}(2p^2)$, leading to the state $He^+(2p)$ + $He^+(2p)$. In Fig. 7(a), we also display angular differential cross sections for TE into $(2s,2s)$, $(2p,2p)$ and $(2s,2p)\&(2p,2s)$ channels obtained from present SCASCC calculations at 30 keV/u. It can be seen that significant contributions from large projectile scattering angles appear for all the three channels, which may suggest that both the small internuclear distance radial coupling and rotational coupling at the united-atom limit are responsible for the large angle scattering mechanism at 30 keV/u.

## V. CONCLUSIONS

In conclusion, we have presented a systematic comparison of experimental data and theories for angular-differential cross sections of electron capture in 30-125 keV/u $He^{2+}$ + He collisions. Employing high-resolution longitudinal cold target recoil ion momentum spectroscopy (COLTRIMS), we successfully acquired high-resolution ngitudinal momentum spectra. The precise $n$-resolved relative state-selective cross sections obtained in the present experiment provide experimental benchmarks available for the development of multi-electrons semiclassical or quantum calculation. In the projectile angular-differential cross sections, overall good agreements were also obtained between the present experimental and theoretical results. It is shown that the GT process mainly occurs at small projectile scattering angles within 0.4 mrad, where prominent oscillatory structures can be observed. We have shown that these oscillatory structures are stemming from the atomic matter-wave Fraunhofer-type diffraction. For ET to higher excited states, the cross sections show similar structures as in GT processes. Furthermore, a significant contribution from large projectile scattering angles (> 0.6 mrad) was observed from both the present experimental and theoretical results for TE process at 30 keV/u. From a quasimolecular interaction picture, it may suggests that both the radial coupling at the small internuclear distance and rotational coupling at the united-atom limit are responsible for the latter mechanism.

## ACKNOWLEDGMENT

This work was supported by Young Scholars in Western China of Chinese Academy of Sciences (2021), and the National Natural Science Foundation of China (Grant No.s 11804347, U1832201, and 12374229). Many thanks are given to the engineers who operated the 320-kV platform for their assistance in running the ECR ion source.

[1] Bransden B H and McDowell M R C 1992 *Charge Exchange and the Theory of Ion-Atom Collisions* (Oxford University, London)
[2] Massey H S W, McDaniel E W and Bederson B 1982 *Applied Atomic Collision Physics Vol 1* (Academic, San Diego)
[3] Cravens T E 2002 *Science* **296** 1042–1045 URL https://www.science.org/doi/abs/10.1126/science.1070001
[4] Otranto S, Olson R E and Beiersdorfer P 2007 *J. Phys. B: At. Mol. Opt. Phys.* **40** 1755–1766 URL https://doi.org/10.1088/0953-4075/40/10/010
[5] Bodewits D, Hoekstra R, Seredyuk B, McCullough R W, Jones G H and Tielens A G G M 2006 *Astrophys. J.* **642** 593–605 URL https://doi.org/10.1086/500731
[6] Greenwood J B, Chutjian A and Smith S J 2000 *Astrophys. J.* **529** 605–609 URL https://doi.org/10.1086/308254
[7] Balsiger H, Altwegg K, Bühler F, Geiss J, Ghielmetti A G, Goldstein B E, Goldstein R, Huntress W T, Ip W H, Lazarus A J, Meier A, Neugebauer M, Rettenmund U, Rosenbauer H, Schwenn R, Sharp R D, Shelley E G, Ungstrup E and Young D T 1986 *Nature* **321** 330–334 URL https://doi.org/10.1038/321330a0
[8] Gervais B, Beuve M, Olivera G and Galassi M 2006 *Radiat. Phys. Chem.* **75** 493–513 ISSN 0969-806X URL https://www.sciencedirect.com/science/article/pii/S0969806X05002616
[9] Fischer D, Feuerstein B, DuBois R D, Moshammer R, López-Urrutia J R C, Draganic I, Lörch H, Perumal A N and Ullrich J 2002 *J. Phys. B: At. Mol. Opt. Phys.* **35** 1396–1377 URL https://iopscience.iop.org/article/10.1088/0953-4075/35/5/318
[10] Gegier H and Marsden E 1909 *Proc. Roy. Soc. London Ser. A* **82** 495–500 URL https://royalsocietypublishing.org/doi/10.1098/rspa.1909.0054
[11] Stolterfoht N, DuBois R D and Rivarola R D 1997 *Electron Emission in Heavy Ion-Atom Collisions* (Springer, Berlin)
[12] Schöffler M S, Titze J N, Schmidt L P H, Jahnke T, Jagutzki O, Schmidt-Böcking H and Dörner R 2009 *Phys. Rev. A* **80**(4) 042702 URL https://link.aps.org/doi/10.1103/PhysRevA.80.042702
[13] Guo D L, Ma X, Zhang S F, Zhu X L, Feng W T, Zhang R T, Li B, Liu H P, Yan S C, Zhang P J and Wang Q 2012 *Phys. Rev. A* **86**(5) 052707 URL https://link.aps.org/doi/10.1103/PhysRevA.86.052707
[14] Zhang R T, Zhu X L, Li X Y, Liu L, Zhang S F, Feng W T, Guo D L, Gao Y, Zhao D M, Wang J G and Ma X 2017 *Phys. Rev. A* **95**(4) 042702 URL https://link.aps.org/doi/10.1103/PhysRevA.95.042702
[15] Zapukhlyak M, Kirchner T, Hasan A, Tooke B and Schulz M 2008 *Phys. Rev. A* **77**(1) 012720 URL https://link.aps.org/doi/10.1103/PhysRevA.77.012720
[16] Dörner R, Ullrich J, Schmidt-Böcking H and Olson R E 1989 *Phys. Rev. Lett.* **63**(2) 147–150 URL https://link.aps.org/doi/10.1103/PhysRevLett.63.147
[17] Puckett L J and Martin D W 1970 *Phys. Rev. A* **1**(5) 1432–1439 URL https://link.aps.org/doi/10.1103/PhysRevA.1.1432
[18] Mančev I, Milojević N and Belkić D c v 2012 *Phys. Rev. A* **86**(2) 022704 URL https://link.aps.org/doi/10.1103/PhysRevA.86.022704
[19] Zajfman D and Maor D 1986 *Phys. Rev. Lett.* **56**(4) 320–323 URL https://link.aps.org/doi/10.1103/

PhysRevLett.56.320

[20] Winter T G 1991 *Phys. Rev. A* **44**(7) 4353–4367 URL https://link.aps.org/doi/10.1103/PhysRevA.44.4353

[21] Belkić D 1988 *Phys. Rev. A* **37**(1) 55–67 URL https://link.aps.org/doi/10.1103/PhysRevA.37.55

[22] Hvelplund P, Heinemeier J, Pedersen E H and Simpson F R 1976 *J. Phys. B: Atom. Mol. Phys.* **9** 491–496 URL https://doi.org/10.1088/0022-3700/9/3/017

[23] Shah M B and Gilbody H B 1985 *J. Phys. B: Atom. Mol. Phys.* **18** 899–913 URL https://doi.org/10.1088/0022-3700/18/5/010

[24] DuBois R D 1987 *Phys. Rev. A* **36**(6) 2585–2593 URL https://link.aps.org/doi/10.1103/PhysRevA.36.2585

[25] de Castro Faria N V, Freire F L and de Pinho A G 1988 *Phys. Rev. A* **37**(1) 280–283 URL https://link.aps.org/doi/10.1103/PhysRevA.37.280

[26] Shah M B, McCallion P and Gilbody H B 1989 *J. Phys. B: Atom. Mol. Phys.* **22** 3037 URL https://dx.doi.org/10.1088/0953-4075/22/19/018

[27] Gramlich K, Grün N and Scheid W 1989 *J. Phys. B: At. Mol. Opt. Phys.* **22** 2567–2579 URL https://doi.org/10.1088/0953-4075/22/16/014

[28] Kimura M 1988 *J. Phys. B: At. Mol. Opt. Phys.* **21** L19–L24 URL https://doi.org/10.1088/0953-4075/21/2/005

[29] Singal R and Lin C D 1991 *J. Phys. B: At. Mol. Opt. Phys.* **24** 251–264 URL https://doi.org/10.1088/0953-4075/24/1/025

[30] Mančev I 1999 *Phys. Rev. A* **60**(1) 351–358 URL https://link.aps.org/doi/10.1103/PhysRevA.60.351

[31] Mančev I 2002 *J. Phys. B: At. Mol. Opt. Phys.* **36** 93–104 URL https://doi.org/10.1088/0953-4075/36/1/307

[32] Mančev I and Milojević N 2010 *Phys. Rev. A* **81**(2) 022710 URL https://link.aps.org/doi/10.1103/PhysRevA.81.022710

[33] Dunseath K M and Crothers D S F 1991 *J. Phys. B: At. Mol. Opt. Phys.* **24** 5003 URL https://dx.doi.org/10.1088/0953-4075/24/23/026

[34] Abufager P N, Martínez A E, Rivarola R D and Fainstein P D 2004 *J. Phys. B: At. Mol. Opt. Phys.* **37** 817 URL https://dx.doi.org/10.1088/0953-4075/37/4/009

[35] Afrosimov V V, Basalaev A A, Leiko G A and Panov M N 1978 *Sov. Phys. JETP* **47** 5 URL http://www.jetp.ras.ru/cgi-bin/dn/e_047_05_0837.pdf

[36] Folkerts H O, Bliek F W, Meng L, Olson R E, Morgenstern R, Hellermann M V V, Summers H P and Hoekstra R 1994 *J. Phys. B: At. Mol. Opt. Phys.* **27** 3475–3488 URL https://doi.org/10.1088/0953-4075/27/15/022

[37] Mergel V, Dörner R, Ullrich J, Jagutzki O, Lencinas S, Nüttgens S, Spielberger L, Unverzagt M, Cocke C L, Olson R E, Schulz M, Buck U, Zanger E, Theisinger W, Isser M, Geis S and Schmidt-Böcking H 1995 *Phys. Rev. Lett.* **74**(12) 2200–2203 URL https://link.aps.org/doi/10.1103/PhysRevLett.74.2200

[38] Dörner R, Mergel V, Jagutzki O, Spielberger L, Ullrich J, Moshammer R and Schmidt-Böcking H 2000 *Phys. Rep.* **330** 95–192 ISSN 0370-1573 URL https://www.sciencedirect.com/science/article/pii/S037015739900109X

[39] Ullrich J, Moshammer R, Dorn A, Dörner R, Schmidt L P H and Schmidt-Böcking H 2003 *Rep. Prog. Phys.* **66** 1463–1545 URL https://doi.org/10.1088/0034-4885/66/9/203

[40] Schöffler M S, Titze J, Schmidt L P H, Jahnke T, Neumann N, Jagutzki O, Schmidt-Böcking H, Dörner R and Mančev I 2009 *Phys. Rev. A* **79**(6) 064701 URL https://link.aps.org/doi/10.1103/PhysRevA.79.064701

[41] Alessi M, Otranto S and Focke P 2011 *Phys. Rev. A* **83**(1) 014701 URL https://link.aps.org/doi/10.1103/PhysRevA.83.014701

[42] Xiao-Long Z, Xin-Wen M, Bin L, Hui-Ping L, Lan-Fang C, Shao-Feng Z, Dong-Bin Q, Wen-Tian F, Shi-Ping C, Shan S and Da-Cheng Z 2006 *Chin. Phys. Lett.* **23** 587 URL https://dx.doi.org/10.1088/0256-307X/23/3/017

[43] Wang Q, Ma X, Zhu X L and Zhang S F 2011 *J. Phys. B: At. Mol. Opt. Phys.* **45** 025202 URL https://doi.org/10.1088/0953-4075/45/2/025202

[44] Ma X, Liu H P, Sun L T, Song M T, Zhu X L, Sha S, Feng W T, Zhang D C, Zhang S F, Li B, Li J Y, Qian D B, Xu S Y, Gao D Q, Wang P Z, Ma L Z, Man K D, Xiao G Q, Zhao H W and Zhan W L 2009 *J. Phys: Conf. Ser.* **163** 012104 URL https://doi.org/10.1088/1742-6596/163/1/012104

[45] Ma X, Zhang R T, Zhang S F, Zhu X L, Feng W T, Guo D L, Li B, Liu H P, Li C Y, Wang J G, Yan S C, Zhang P J and Wang Q 2011 *Phys. Rev. A* **83**(5) 052707 URL https://link.aps.org/doi/10.1103/PhysRevA.83.052707

[46] Gao Y, Cao T, Lin K Z, Guo D L, Zhang S F, Zhu X L, Zhang R T, Yan S C, Xu S, Zhao D M and Ma X 2024 *Rev. Sci. Instrum.* **95** 043302

[47] Cao T, Meng T, Gao Y, Zhang S F, Zhang R T, Yan S, Zhu X L, Wang J, Ma P, Ren B, Xia Z H, Guo D L, Zhang C J, Lin K Z, Xu S, Wei B and Ma X 2023 *Astrophys. J. Suppl. Ser.* **266** 20 URL https://doi.org/10.3847/1538-4365/accba2

[48] Wiley W C and McLaren I H 1955 *Rev. Sci. Instrum.* **26** 1150–1157 URL https://doi.org/10.1063/1.1715212

[49] Guo D L, Gao J W, Zhang S F, Zhu X L, Gao Y, Zhao D M, Zhang R T, Wu Y, Wang J G, Dubois A and Ma X 2021 *Phys. Rev. A* **103**(3) 032827 URL https://link.aps.org/doi/10.1103/PhysRevA.103.032827

[50] Guo D L, Ma X, Zhang R T, Zhang S F, Zhu X L, Feng W T, Gao Y, Hai B, Zhang M, Wang H B and Huang Z K 2017 *Phys. Rev. A* **95**(1) 012707 URL https://link.aps.org/doi/10.1103/PhysRevA.95.012707

[51] Zhang Y W, Gao J W, Wu Y, Wang J G, Sisourat N and Dubois A 2022 *Phys. Rev. A* **106**(4) 042809 URL https://link.aps.org/doi/10.1103/PhysRevA.106.042809

[52] Gao J W, Wu Y, Sisourat N, Wang J G and Dubois A 2017 *Phys. Rev. A* **96**(5) 052703 URL https://link.aps.org/doi/10.1103/PhysRevA.96.052703

[53] Sisourat N, Pilskog I and Dubois A 2011 *Phys. Rev. A* **84** 052722 URL http://adsabs.harvard.edu/cgi-bin/nph-data_query?bibcode=2011PhRvA..84e2722S&link_type=EJOURNAL

[54] Dubois A, Nielsen S E and Hansen J P 1993 *J. Phys. B* **26** 705–721

[55] Gao J W, Wu Y, Wang J G, Sisourat N and Dubois A 2018 *Phys. Rev. A* **97** 052709 URL http://adsabs.harvard.edu/cgi-bin/nph-data_query?bibcode=2018PhRvA..97e2709G&link_type=EJOURNAL

[56] Piacentini R and Salin A 1977 *Compul. Phys. Commun.* **13** 57 – 62 ISSN 0010-4655 URL http://www.sciencedirect.com/science/article/pii/0010465577900273

[57] Agueny H 2015 *Phys. Rev. A* **92**(1) 012702 URL https://link.aps.org/doi/10.1103/PhysRevA.92.012702

[58] Nielsen S E, Rod T H, Salgado J, Dowek D, Houver J C, Thomsen J W and Andersen N 2004 *J. Phys. B: At. Mol. Opt. Phys.* **37** 2119–2133 URL https://doi.org/10.1088/0953-4075/37/10/009

[59] van der Poel M, Nielsen C V, Gearba M A and Andersen N 2001 *Phys. Rev. Lett.* **87**(12) 123201 URL https://link.

aps.org/doi/10.1103/PhysRevLett.87.123201
[60] van der Poel M, Nielsen C V, Rybaltover M, Nielsen S E, Machholm M and Andersen N 2002 *J. Phys. B: At. Mol. Opt. Phys.* **35** 4491–4505 URL https://doi.org/10.1088/0953-4075/35/21/312
[61] Gudmundsson M, Fischer D, Haag N, Johansson H A B, Misra D, Reinhed P, Schmidt-Böcking H, Schuch R, Schöffler M, Støchkel K, Schmidt H T and Cederquist H 2010 *J. Phys. B: At. Mol. Opt. Phys.* **43** 185209 URL https://doi.org/10.1088/0953-4075/43/18/185209
[62] Born M and Wolf E 2000 *Principles of optics: electromagnetic theory of propagation, interference and diffraction of light* (CUP Archive)
[63] Bordenave-Montesquieu D and Dagnac R 1992 *J. Phys. B: At. Mol. Opt. Phys.* **25** 2573–2586 URL https://doi.org/10.1088/0953-4075/25/11/012